PAPER

Polydopamine–cellulose nanofiber composite for flexible electrode material

To cite this article: Ruth M Muthoka et al 2021 Smart Mater. Struct. 30 035025

View the <u>article online</u> for updates and enhancements.

Smart Mater. Struct. 30 (2021) 035025 (11pp)

https://doi.org/10.1088/1361-665X/abe184

Polydopamine—cellulose nanofiber composite for flexible electrode material

Ruth M Muthoka¹, Sunanda Roy¹, Hyun Chan Kim¹, Hargsoon Yoon², Lindong Zhai¹ and Jaehwan Kim¹

E-mail: jaehwan@inha.ac.kr

Received 25 August 2020, revised 23 January 2021 Accepted for publication 29 January 2021 Published 12 February 2021



Abstract

This research is intended to develop a flexible and dopamine-based electrode material by blending polydopamine (PDA) with cellulose nanofiber (CNF). Inspired by its unique adhesion behavior, dopamine, a biomimetic protein, was utilized to form a strong adhesion between the CNFs. Herein, we report PDA concentration's effect to produce PDA-CNF composite showing good electrochemical redox response, good mechanical properties, and improved thermal stability. The PDA-CNF composite with CNF:PDA = 5:2.5 showed the highest Young's modulus, the strain at break, and toughness among other CNF:PDA combination composites. A PDA-CNF working electrode was made using a microfabrication process. Cyclic voltammetry analysis showed high ion permeability through the CNF backbone structure and oxidation process by PDA in PDA-CNF electrode. These findings indicate the feasibility of the PDA-CNF composite for enhanced longevity in flexible electrode applications utilizing the combination of high mechanical flexibility and thermal stability.

Keywords: cellulose, polydopamine, electrode, microfabrication, flexible

(Some figures may appear in colour only in the online journal)

1. Introduction

Neural interface technology for sensing the electrical brain signals and stimulating the brain has attracted clinical applications and scientific interests. An electrode as the neural interface is the most critical part in sensing neural activities and stimulating neural cells [1]. Implantable electrodes are surgically implanted on the cortex's surface or penetrated the brain to sense electrical brain signals or transmit stimuli into the brain. Metal-based implantable electrodes have been used for more than 60 years owing to their advantages of non-toxicity, low impedance, high signal to noise ratio, and better mechanical properties for penetrating the brain. However, they have a chronic reaction associated with dissolution by the tissue fluids and inflammatory reaction.

Metal-based implantable electrodes have been used for more than 60 years owing to their advantages of non-toxicity, low impedance, high signal to noise ratio, and better mechanical properties for penetrating the brain. However, they have a chronic reaction associated with dissolution by the tissue fluids and inflammatory reaction [2]. Even with a successful implementation of neural sensing electrodes in the brain, it has chronic neural recording's longevity issues. The recording capabilities of electrodes have been mostly limited to a few months; they then degrade over time due to neuronal cell degeneration and cell layer formation on the electrodes from the inflammatory immune response caused by the chronic implantation operation [3, 4]. During chronic recording, the brain is subjected to movement brought upon by external motion of the body. The difference in material stiffness between the brain and the electrode makes the brain microvasculature and neural cells more susceptible to mechanical damage such as glial scarring. To mitigate the damages, it is advantageous to use a flexible electrode and

¹ Creative Research Center for Nanocellulose Future Composites, Department of Mechanical Engineering, Inha University, Incheon 22212, Republic of Korea

² Department of Engineering, Norfolk State University, Norfolk, VA 23504, United States of America

ultimately enhance the electrode longevity and to mediate tissue and cell damage from mechanical motion in the brain [5]. Flexible materials-based electrodes have been developed using Parylene-C, polyimide, polydimethylsiloxane, SU-8, benzocyclobutene, and liquid crystal polymer [6–11]. The development of new materials and novel devices for recording and manipulating neural activity is critically important to enable a transformative understanding of dynamic signaling in the brain. Efforts have been made to enhance chronic neural recordings' yield and longevity by applying functional materials [12-15]. By rapid progress in neural probing device technologies, unit spike and multi-neural ensemble recording could be available over a long time [16, 17]. Thus, flexible and biocompatible electrode materials are necessary to enhance the electrode longevity and mitigate inflammatory reactions, applied for human physiological monitoring, drug delivery, energy harvesting garment from body movement, and motion sensors [18-21].

While the industrial development of plastic in many ways made life easier and comfortable, the decomposition of plastics has become a serious global concern. The decomposition of plastics like polyvinyl chloride (PVC), polypropylene (PP), polyethylene (PE), polyethylene terephthalate (PET), and many others consumes a lot of energy and produces substantial greenhouse gases. Therefore, there is a growing demand for alternative sustainable materials with similar or superior properties. In this context, cellulose, the most abundant natural polymer on earth, is attractive for its biocompatible, renewable, and cost-effective behaviors [22, 23]. Cellulose can be found naturally in plant cells such as wood and cotton or various bacterial species, algae, and fungi. Among them, wood-based cellulose is the most common and preferred one, as it is readily available in the form of pulp fibers. By mechanical or chemical treatment, the pulp fibers can be transformed into cellulose nanofibers (CNFs) or cellulose nanocrystals (CNCs) that possess outstanding flexibility, transparency, and mechanical properties as compared with the original cellulosic fiber. Not only that, crystalline cellulose is found to be even stronger than Kevlar fiber or steel wires and Young's modulus of CNF of wood pulp is about 90-110 GPa [24, 25]. Cellulose contains many hydroxyl groups, which allow in forming intermolecular or intramolecular hydrogen bonds between fibers or within fibers [22, 24] and easy chemical modification for improving functional properties. Cellulose has become an attractive and alternative candidate for new generation structural and functional applications, including neural interfacing substrate [26–33]. In this article, CNF is used for the flexible electrode substrate owing to its flexibility, mechanical properties, and biocompatibility.

However, the CNF-based flexible electrode should have unique surface characteristics that will enhance the electrode longevity and mitigate inflammatory reactions. In recent years, mussel adhesive proteins have drawn an interest in the research community for their unique ability to form strong bonds between the mussel and various substrates. It was found that 3,4-dihydroxyphenyl-1-alanine (DOPA), the critical element of mussel adhesive proteins, is responsible for the adhesive properties between the mussels and substrates

[34, 35]. Inspired by the structure of DOPA, a dopamine coating having the same functional unit as is in the mussel adhesive proteins has been developed, which can selfpolymerize under mild alkaline conditions and generate polydopamine (PDA) coating layer onto almost all types of materials including glass, ceramics, plastics, metals, and semiconductors [36]. PDA coating has been extensively reported in numerous articles for nanofiller and modifier of bulk nanocomposites, a corrosion protection layer, antifouling supporting layer, stem cell growth, biosensors, and wastewater purification [37-42]. Modification of CNF by PDA has been of particular interest for many areas, including oxidative polymerization coating, mechanical properties improvement, flame-retardant composites, caffeine removal, organic dyes removal, Cr(VI) ion removal, oil-separation, enhanced scaffolds, drug delivery, photo-degradation performance, and contaminants removal from water [43–53]. Recently, researchers are focused on exploiting the various unique properties of PDA on cellulose-based composites.

Inspired by PDA's benefits, in this article, CNF was blended with PDA to improve further the composite's mechanical and electrochemical properties, suitable for flexible electrodes that will enhance the longevity and mitigate inflammatory reactions. A novel strategy to develop a flexible and functionally stable PDA-CNF (P-CNF) composite is made with controlled PDA adhesion. The PDA effect is investigated on the physical, mechanical, thermal, and electrochemical behaviors of P-CNF composites. As the PDA adhesion in the P-CNF composite depends on the dopamine polymerization, P-CNF composite characteristics can be altered depending on the dopamine concentration and reaction time. These effects were reflected in the physio-mechanical properties of the prepared P-CNF composite. The P-CNF composite will be useful for flexible electrodes in many biomedical applications [48, 51, 54–56].

2. Materials and methods

2.1. Materials

Dopamine hydrochloride and Trizma base (≥99.9% purity) were purchased from Sigma Aldrich, South Korea. The cellulose nanofibers (CNFs) used here was isolated from hardwood kraft pulp received from Chungnam National University, South Korea (original source from Canada). Tris buffer consisting of 10 mM Tris (pH 8.1) was used for all the experiments. The buffer solutions were made with ultrapure water (Milli-Q gradient).

2.2. Preparation of P-CNF composite

Before using CNFs for preparing P-CNF composite, they were isolated by using the combination of 2,2,6,6-tetramethylpiperidine-1-oxyl radical (TEMPO) oxidation and aqueous counter collision (ACC) methods [57–62]. The hardwood pulp was oxidized with TEMPO, 98% oxidized for 60 min, and then subjected to 30 times ACC process to obtain

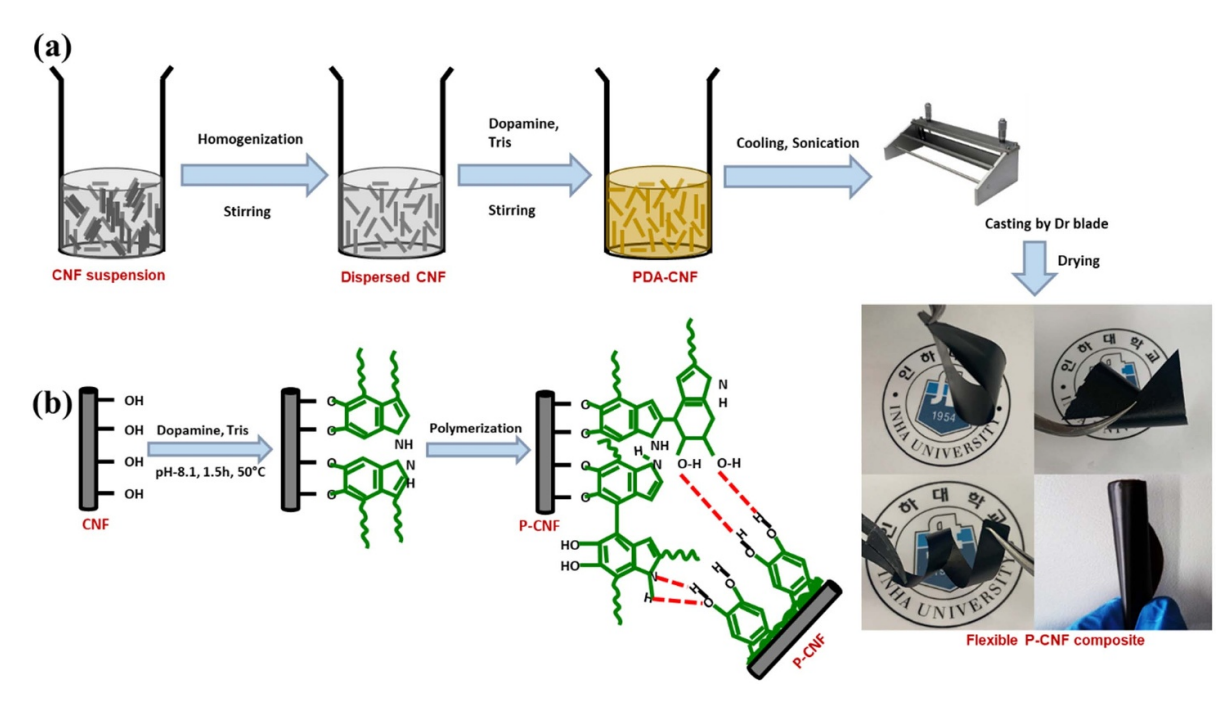


Figure 1. Schematic diagrams for the P-CNF composite preparation: (a) the preparation procedure and (b) the reaction scheme of PDA and CNF.

fine nanofibers. The P-CNF composite was fabricated as follows: 50 ml of 1% concentration TEMPO-oxidized CNF suspension (contained 500 mg CNF) was homogenized for 5 min at 1000 rpm followed by magnetic stirring at 500 rpm for 15 min. Hundred milligrams of dopamine hydrochloride was dissolved in 5 ml of 10 mM Tris buffer solution and immediately added into the above CNF suspension to make a CNF:PDA ratio of 5:1. The mixture was then stirred vigorously at 500 rpm and 50 °C for 1.5 h to allow the polymerization process. Finally, after cooling under the sonication bath, the mixture was cast on a polycarbonate substrate using a doctor blade, followed by air drying. The composite was detached from the substrate with the help of ethanol. The fabrication process of the P-CNF composite and the corresponding reaction scheme is shown in figure 1.

More P-CNF composites with CNF:PDA ratio of 5:2.5 and 5:3.5 were prepared using the same procedure under identical conditions by varying PDA concentration. For simplicity, we named the three composites as P-CNF1, P-CNF2, and P-CNF3 where, 1, 2, and 3 represent the CNF-PDA composite ratio (5:1, 5:2.5 and 5:3.5), respectively. This method of preparing P-CNF composites by casting produced composites with even thickness throughout, approximately 14 μ m.

2.3. Characterization

Surface chemical composition analysis of all P-CNF composites and the pure CNF was carried out using a Fourier transform infrared spectroscopy (FTIR, Excalibur FTS 3000, Bio-Rad, Hercules, USA) at 16 scan rate with 4 cm⁻¹ resolution. The elemental compositions of the composites were determined by x-ray photoelectron spectroscopy (XPS) on a K-Alpha Thermo scientific spectrometer with monochromatic

Al K α x-ray radiation. All XPS spectra were corrected according to the C1s line at 284.8 eV. The cross-sectional morphologies of the tensile fractured composites were analyzed using a field emission scanning electron microscope (FESEM, Hitachi S4200, Tokyo, Japan). The thermal properties were investigated with thermogravimetric analysis (TGA) TG 209 F3 Tarsus equipment over a temperature range from 30 °C to 600 °C under nitrogen at a heating rate of 10 °C min⁻¹. The tensile test was performed with a custom tensile testing system [32]. Specimens were cut into dimensions of 60×10 mm. The gauge length of the samples was 40 mm, and the applied pulling rate was 0.005 mm s⁻¹. Five samples for each condition (100 mg, 250 mg, and 350 mg PDA) were measured, and the averaged values were used to approximate the corresponding mechanical properties of the P-CNF composites. A reference specimen was prepared using the pure CNF suspension.

2.4. Electrochemical characterization

The electrochemical response of the P-CNF composites was investigated by conducting cyclic voltammetry (CV) using an electrochemical interface, Solartron SI 1287. The electrochemical experiments were conducted with a three-electrode system. In this case, a platinum plate served as the counter electrode, and an Ag/AgCl reference electrode filled with 3 M KCl solution from Sigma Aldrich was applied. Platinum electrodes covered with pure CNF, PDA, and P-CNF composites were used as the working electrode in experiments. The CV tests were performed under a voltage ramp in the range -0.8 to 0.8 V at various scan rates in phosphate-buffered saline (PBS). All the CV experiments were conducted at room temperature.

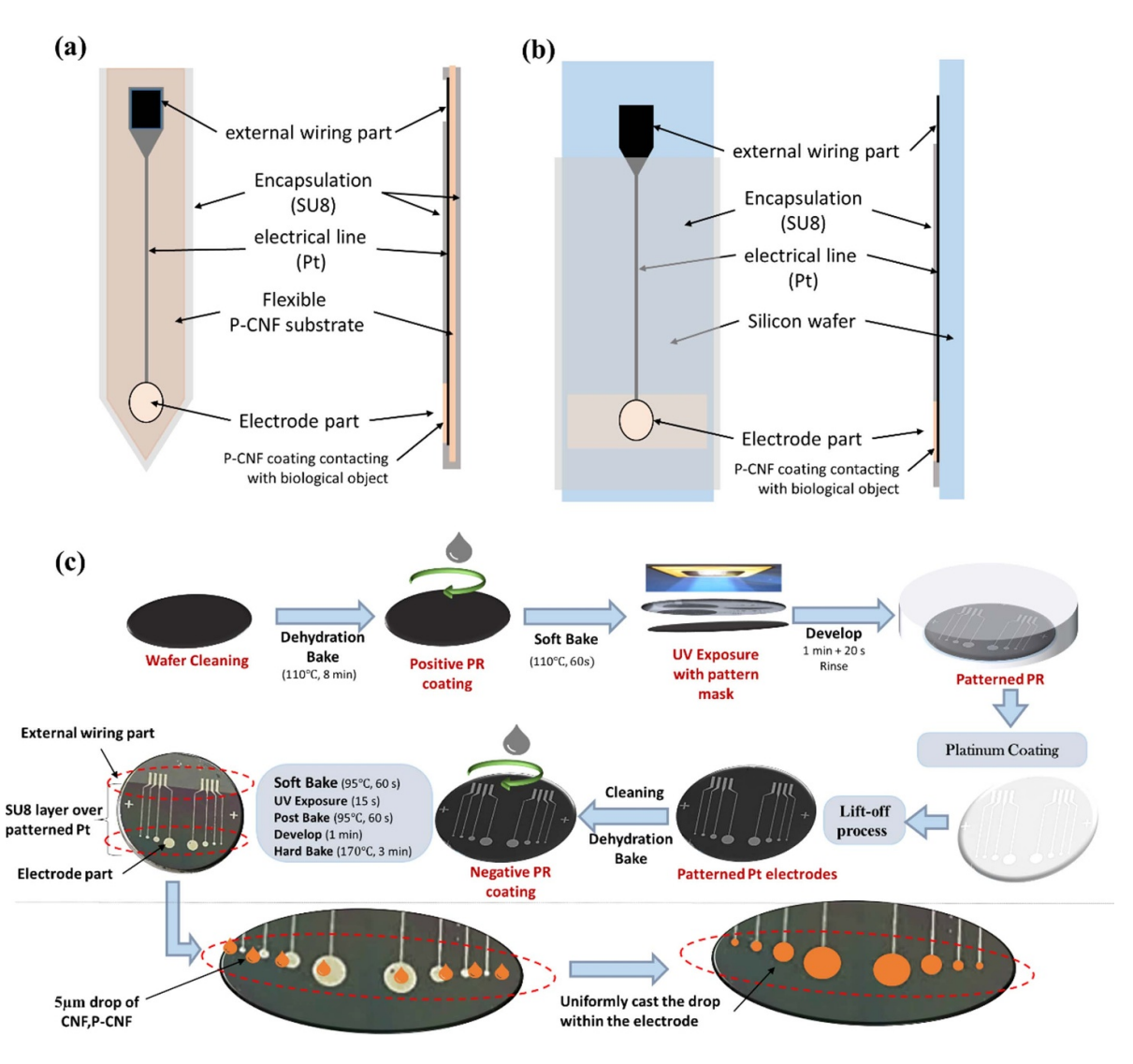


Figure 2. (a) The flexible electrode concept made of P-CNF composite, (b) the P-CNF electrode implemented on a silicon wafer for CV measurement, (c) fabrication process of the P-CNF composite working electrode for CV measurement.

The working electrode is very important to measure the electrochemical behaviors of the composites consistently. Figure 2(a) shows the flexible electrode concept made of P-CNF composite. However, it is not easy to fabricate because the Pt electrical line and electrode deposition, encapsulation, and electrode zone elimination are complicated in fabrication. Thus, before implementing the flexible P-CNF electrode, we primarily implemented the electrode on a silicon wafer instead of a P-CNF flexible substrate, shown in figure 2(b), and performed its CV measurement. It can easily be fabricated, and stable CV results are expected.

The working electrodes were fabricated on a silicon wafer by a micro-fabrication process. Figure 2(c) shows the fabrication process. Four different working electrode sizes were designed and fabricated to characterize the electrochemical properties of the P-CNF composites. A two-step lithography technique was used. The first lithography process was applied to pattern the platinum working electrode array on a silicon wafer using a positive photoresist (PR). A lift-off process was used to fabricate the platinum electrode array. The second

lithography was then applied using a negative PR (SU8) to selectively make the circular electrode parts and the external wiring parts. The silver paste was used for copper wiring to the external wiring parts for CV measurement. A thin layer of P-CNF suspension was dropped and cast over the patterned-platinum layer and left out overnight to dry at 40 °C. The electrodes array covered by P-CNF, or CNF depositions were dipped into PBS, and CV tests were performed.

3. Results and discussion

3.1. Surface chemical property of P-CNF

The P-CNF composites were fabricated by blending CNF suspension and PDA, and the corresponding PDA reaction scheme is presented in figure 1. The color change of the composites from clear to dark indicates the oxidative self-polymerization of dopamine hydrochloride. The possible mechanism of the polymerization process has also been

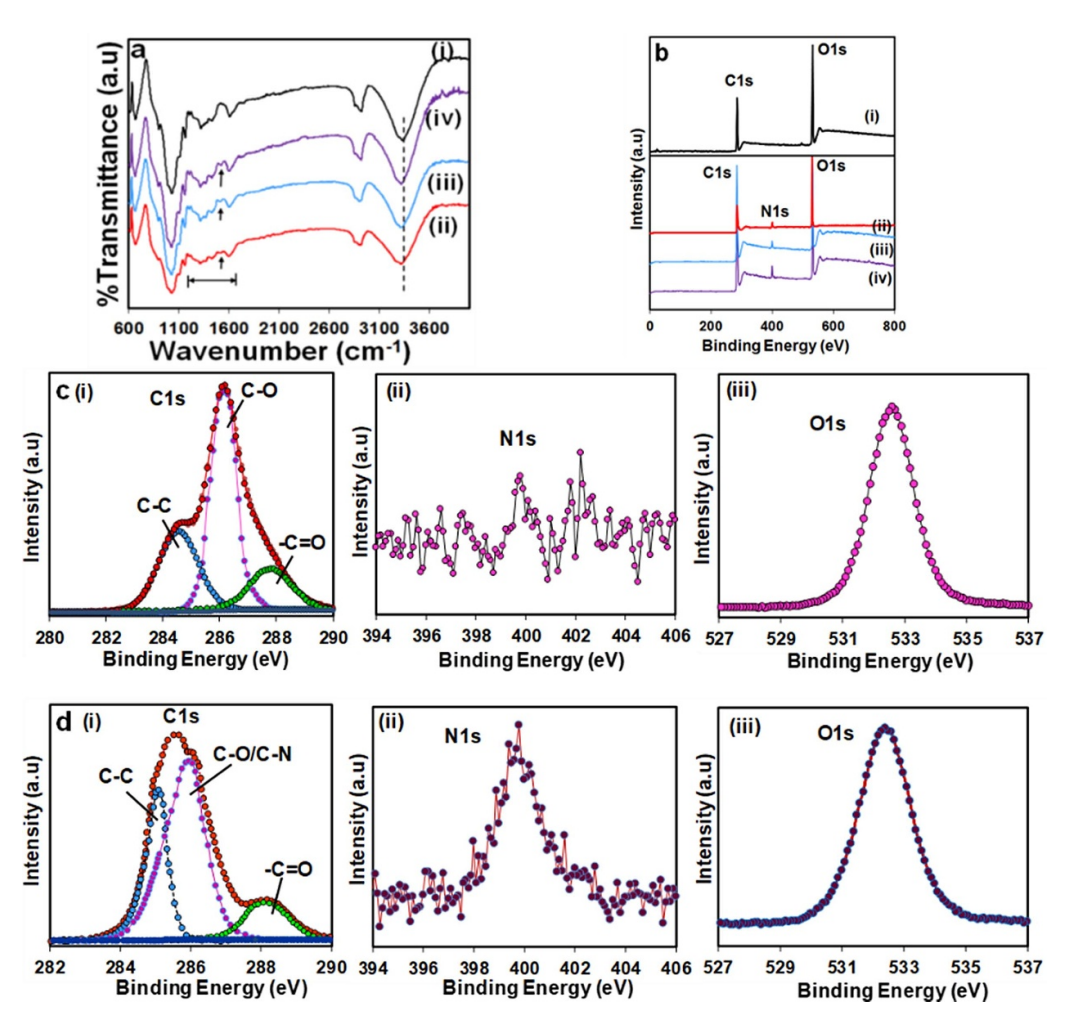


Figure 3. (a) FTIR spectra of pristine CNF (i), P-CNF1 (ii), P-CNF2 (iii), and P-CNF3 (iv) composites; (b) XPS survey spectra of pristine CNF (i), P-CNF1 (ii), P-CNF1 (iii), and P-CNF3 (iv) composites; (c), (d) XPS high-resolution C1s, N1s, and O1s spectra of the pure CNF and P-CNF3 composite, respectively.

Table 1. Summary of the atomic and elemental composition obtained from XPS analysis and thermal decomposition temperature measured from TGA analysis for various cellulose composites.

	Concentrations of chemical species (%)			Atomic concentration (%)			Thermal decomposition temperature	
	284.9 eV	286.2 eV	288.3 eV					
Samples	-C-C-	-C-O-,-C-N-	-C=O	C	O	N	T_5	T_{50}
Pristine CNF	34.78	41.68	23.54	60.73	39.27	_	192	328.1
P-CNF1	34.04	42.26	23.70	57.26	39.65	3.09	191.4	333.6
P-CNF2	33.16	42.85	23.99	56.29	39.98	3.73	191.8	350.3
P-CNF3	30.76	44.71	24.53	55.46	40.41	4.13	196.3	363.5

explained elsewhere [34, 37]. The P-CNF composite can withstand twisting, bending, and folding forces, which illustrates its flexibility.

The successful formation of PDA adhesion on the surface of CNF was verified by FTIR and XPS analysis, as shown in figure 3. Figure 3(a) compares the FTIR spectra of the pure CNF with P-CNF composites. The FTIR spectrum of the pure CNF showed a broad peak around 3150–3620 cm⁻¹ corresponding to the stretching of –OH groups of free alcohol and the hydrogen bonds [32]. The band at 1610 and 1022 cm⁻¹ were

attributed to the characteristic peaks for the O–H bending of absorbed water and C–O–C stretching, respectively [57]. The peak observed between 2840 and 3000 cm⁻¹ assigned to CH-stretching. The FTIR spectra of all P-CNF composites showed almost identical spectral features to that of the pure CNF, but some new absorption peaks have also appeared. The peaks at 1430–1610 cm⁻¹ were attributed to the aromatic ring stretching, and N–H bending vibrations resulted from PDA. The broad peak at 3326 cm⁻¹ was due to the catechol –OH groups and N–H groups [34]. These changes in the FTIR

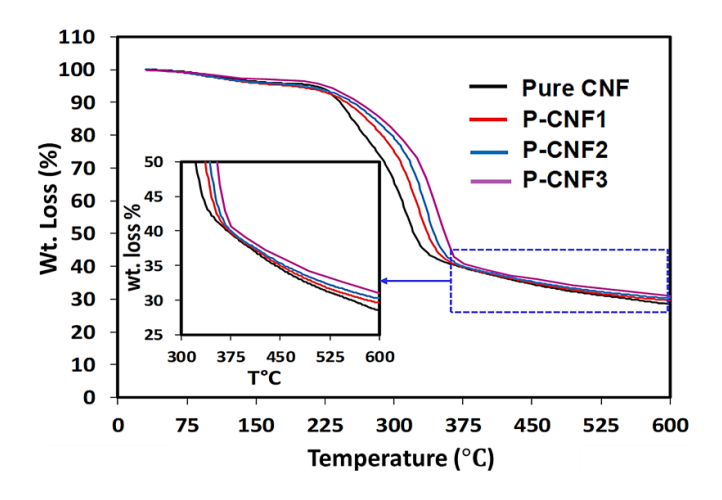


Figure 4. TGA weight loss curves of the pure CNF, P-CNF1, P-CNF2, and P-CNF3 composites.

spectra indicate the presence of PDA on the CNF surface. The intensity increase of the above peaks further demonstrates that the PDA adhered more on the CNF surface as the dopamine concentration increased.

The successful PDA adhesion onto CNF was further ascertained by comparing the XPS spectra of the above composites. Figure 3(b) shows the XPS survey spectra of the pure CNF, P-CNF-1, P-CNF2, and P-CNF3. The XPS spectrum of the pure CNF showed a strong peak at the binding energy (BE) of 284.9 and 532 eV, assigned to C1s and O1s, respectively. However, in P-CNF composites, a clear N1s peak was found at 400 eV, which ascribes to nitrogenated groups' existence on the CNF surfaces. The appearance of N1s peak indicates the successful adhesion of PDA layers on the surface of CNF. It can also be seen from figure 3(b)(ii-iv) that the height of N1s peak increases with increasing the concentrations of PDA, suggesting the adhesion of a higher amount of PDA content as a result of the continuous successful polymerization reaction. Detailed compositions of C, O, and N atoms are given in table 1. An apparent change in carbon bond composition was observed in the high-resolution carbon spectra (C1s), supporting PDA adhesion onto CNF. The high-resolution C1s spectrum of the pure CNF was deconvoluted into three different curves. The BEs centered at 284.9, 286.2, and 288.3 eV are assigned to the carbon skeleton (-C-C-/-C-H-), a hydroxyl group (-C-OH), and carbonyl group (-C=O), respectively (figure 3(c)(i)). The C1s spectrum of modified composite (shown only the profile for P-CNF3 composite) also showed three similar peaks at the same binding energy. Meanwhile, the peak intensities of the -C-O/-C-N and -C=O groups showed significant improvement, suggesting the adhesion of catechol/quinone groups of PDA onto the CNF (see figure 3(d)(i)). The O1s and N1s corelevel spectra for the pure CNF and P-CNF3 composite are presented in figures 3(c) and (d). As the pure CNF does not contain any nitrogen group, therefore no peak for N1s was detected at the BE of 400 eV (figure 3(c)(ii)). The broad and intense O1s peak confirms the ample oxygen content in the pure CNF. For better clarity, the high-resolution O1s and N1s spectra for P-CNF3 composite are also presented in figure 3(d)

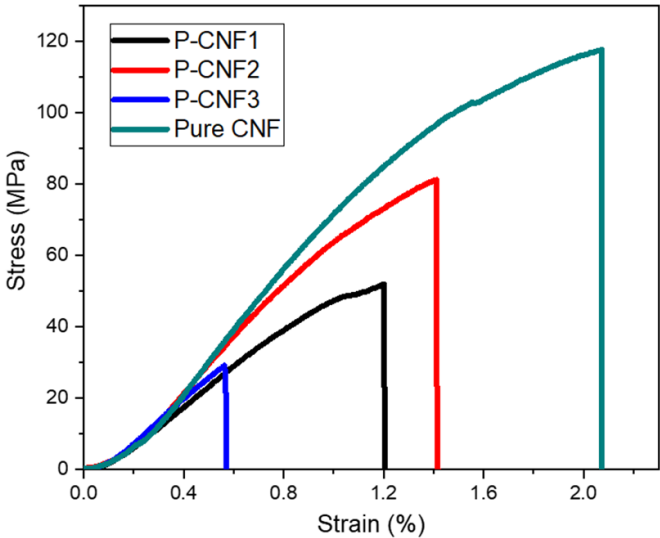


Figure 5. Stress–strain curves of the pure CNF, P-CNF1, P-CNF2, P-CNF3 composites.

(ii) and (iii). As expected, broad peaks for both N1s and O1s have emerged in the XPS profiles. The results shown in table 1 indicate an appreciable increase in the percentage of atomic oxygen and nitrogen for all the modified composites, resulting in a higher –C–O/–C–N and –C=O groups than the pure CNF.

3.2. Thermal stability

Figure 4 shows the TGA curves of pure CNF, P-CNF1, P-CNF2, and P-CNF3 composites. The TGA curves showed that the weight loss of all P-CNF composites occurred in three steps. The initial weight loss between 30 °C and 130 °C was mainly due to the vaporization and weight loss of absorbed water and moisture content in the cellulose. The second weight loss in the region 220 °C-330 °C can be explained due to the cleavage of glycosidic linkages of the cellulose and the decomposition of surface functional groups. The third decomposition was shown at a higher temperature, generally around 350 °C-550 °C. The weight loss in this region is attributed to the degradation of cellulose. The decomposition temperatures at 5% (T_5) and 50% weight loss (T_{50}) are 192 °C and 328.1 °C, respectively, and summarized in table 1. It is exciting to find that the PDA use can significantly delay the decomposition temperature of the CNF to shift to the higher temperature side. It has been reported that PDA exhibits good thermal stability up to 400 °C [35]. Although not much difference was shown at the initial stage of decomposition (at 5% decomposition) between the pure CNF and P-CNF composites but marked increase in the temperature was found at 50% decomposition temperature. It is also apparent that increasing PDA concentration can steadily increase the thermal stability of the composites.

The P-CNF3 composite exhibited the highest thermal stability with an increase of 35.4 °C at T_{50} compared to the pure CNF. No further improvement in the decomposition temperature was noticed beyond P-CNF3 (CNF:PDA = 5:3.5), thus

Toughness (KJ $\,\mathrm{m}^{-3}$) Young's modulus (GPa) Tensile strength (MPa) Strain at break (%) 8.62 ± 0.12 117.72 ± 8.34 2.06 ± 0.21 1380.95 ± 58.60 Pristine CNF P-CNF1 6.22 ± 0.79 55.71 ± 21.96 1.12 ± 0.35 392.09 ± 106.75 79.97 ± 11.68 P-CNF2 6.74 ± 0.40 1.14 ± 0.44 660.58 ± 126.32 P-CNF3 5.52 ± 0.82 18.44 ± 6.98 0.57 ± 0.14 42.99 ± 4.01

Table 2. Mechanical properties of P-CNF composites.

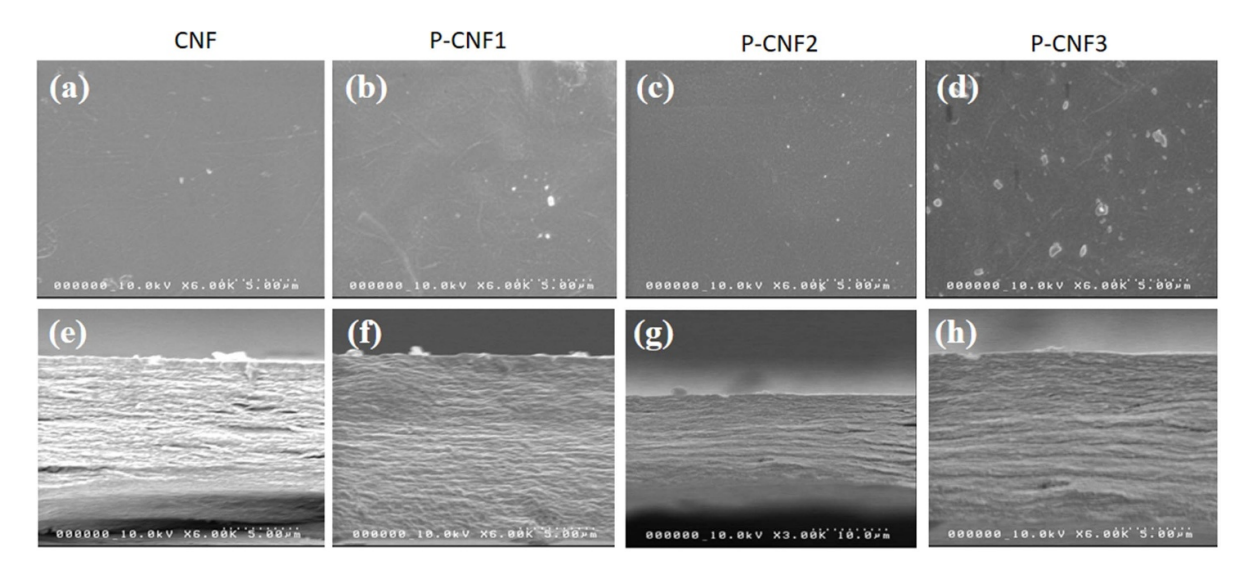


Figure 6. FESEM images: (a)–(d): surface images of the pure CNF, P-CNF1, P-CNF2, and P-CNF3 composites, respectively; (e), (f): cross-sectional images of the pure CNF, P-CNF1, P-CNF2 and P-CNF3 composites, respectively.

not included here. Such a thermal decomposition temperature improvement for P-CNF3 composite might be associated with the strong hydrogen bonds and cross-linked network structure between the CNF and PDA resulting to restricted thermal motion of the cellulose chains at high temperature (see the schematic diagram in figure 1(b)). In addition, the PDA layers within the CNF could impede the onset of degradation of cellulose. It can be an effective physical barrier to prevent the release of volatile products during decomposition. The fiber residue remaining above 550 °C indicates carbonaceous materials in the composite [54].

3.3. Mechanical properties

Figure 5 presents a comparison of the stress–strain curves of the pure CNF and P-CNF composites. From the stress–strain curve, it can be observed that the blending of PDA in CNF exhibited promising mechanical properties. Blending CNF with PDA produced P-CNF composites with Young's modulus values higher than the pristine PDA but lower than the pure CNF sample. The Young's modulus for the pure CNF sample without any stretching or alignment treatment was found to be 8.6 GPa. The pristine PDA exhibits low Young's modulus in the range of 2.0–4.4 GPa, depending on experimental and simulation methods [39, 40, 55]. Table 2 shows the mechanical properties of P-CNF composites.

The flexibility of P-CNF composites is essential for biomedical electrode materials. The flexibility is governed not only by Young's modulus but also its strain at break. The area given by stress-strain curve up to strain at break gives so-called toughness. Toughness is another parameter that indicates the flexibility of the composites. Strain at break and toughness values of prepared composites are shown in table 2. The tensile strength increased from P-CNF1 to P-CNF2 and then decreased again as the concentration increased to P-CNF3. By physical observation, all samples prepared for P-CNF3 presented large amounts of aggregates, while P-CNF2 and P-CNF1 showed small sizes of aggregates that could only be observed by a microscope. A large number of aggregates might be attributed to the low mechanical properties observed at P-CNF3 composite. To verify the PDA aggregation trend, we prepared P-CNF composites with high CNF:PDA ratios, for example, 5:4.5 and 5:5, and more inconsistent aggregates were observed. Hence they were disregarded for the P-CNF composite fabrication. The strain at break increased from P-CNF1 to P-CNF2 and decreased after that, similar to the tensile strength trend. The toughness of the composite was found to be 660.6 kJ m^{-3} for P-CNF2. From the mechanical properties concern, the optimum PDA concentration was found to be at 5:2.5 CNF:PDA concentration that corresponds to P-CNF2.

3.4. Morphology

Based on the mechanical test results, it is necessary to understand the morphologies of the composites. Figure 6 shows the cross-sectional FESEM images of the pure CNF and various P-CNF composites. The cross-sectional fracture surface of the pure CNF is shown in figure 6(a). As can be seen, the fracture

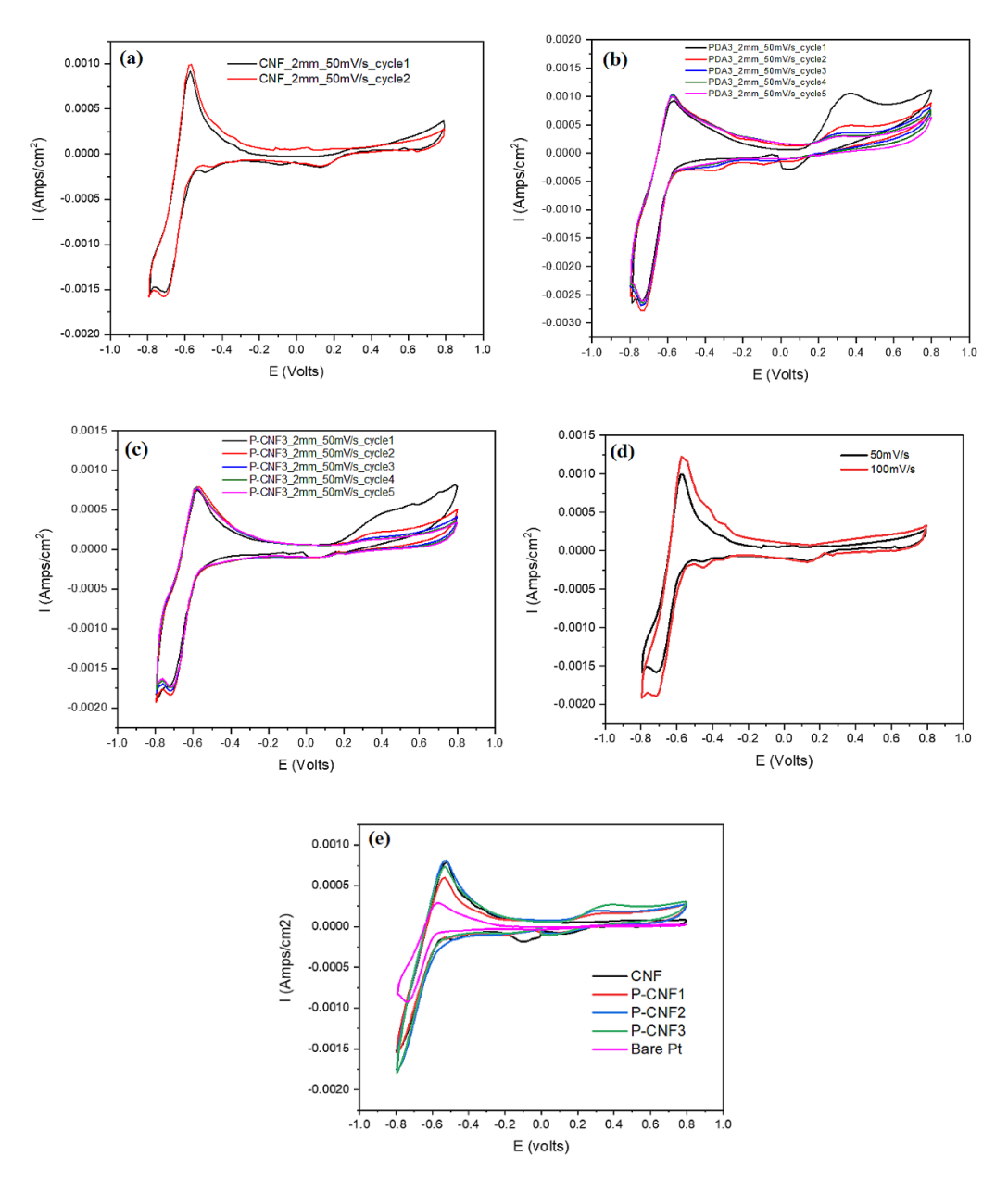


Figure 7. Cyclic voltammetry curves for different surface conditions on 2 mm diameter electrodes: (a) pure CNF, (b) PDA and (c) P-CNF3; (d) different scan rates, 50 and 100 mV s^{-1} , (d) different PDA concentrations: P-CNF1, P-CNF2 and P-CNF3.

edges of all the composites exhibited a compact layer-by-layer stacking structure. However, after modification with PDA, the composites formed a compact and dense layered structure due to the higher hydrogen bonding interactions and unique adhesion of PDA molecules. The compactness increased with increasing the PDA concentration, suggesting more extensive hydrogen-bonding interactions due to more PDA adhesion.

3.5. CV

CV provides information on the electrode and electrolyte interface's charge transfer properties in the presence of electrochemical reactions and their reversibility. In this study, CV was measured to analyze electrochemical properties with different P-CNF depositions. Figures 7(a)–(c) show the CV curves of CNF, PDA, and P-CNF3 depositions on the 2 mm electrode under 50 mV s⁻¹ scanning speed. According to CV measurements, hydrogen adsorption and desorption were commonly observed with similar current densities, which showed hydrogen permeability of CNF, PDA, and P-CNF3 depositions. CV measurements of PDA and P-CNF3 electrodes exhibited dopamine oxidation peaks near 0.4 V, considered electrochemical reactions of dopamine to dopaquinone. As anticipated, the CNF electrode did not show the dopamine oxidation peak. According to the results, it was believed that PDA and residual dopamine in P-CNF depositions were oxidized on the platinum electrode. Note that

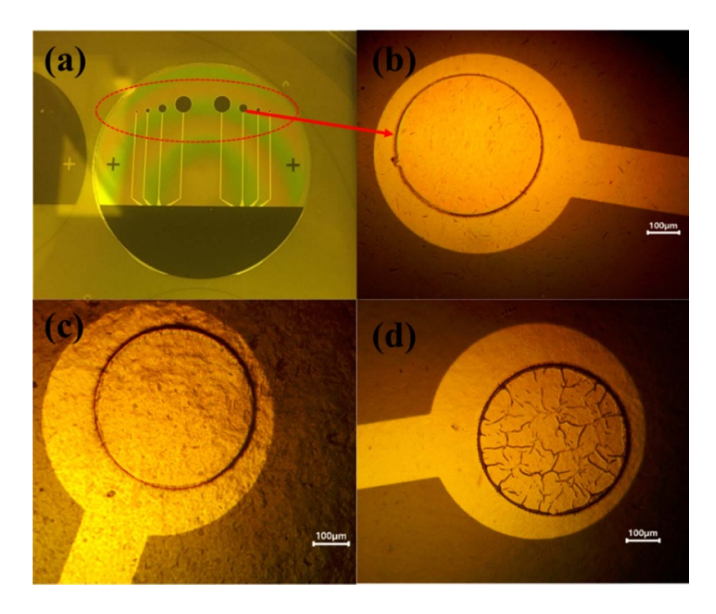


Figure 8. Images of (a) platinum electrodes array, (b) CNF, (c) P-CNF3 electrode before CV analysis, and (d) P-CNF3 electrode after CV analysis in PBS.

the CV curves gradually changed near the oxidation peak as the iteration increases. This irreversible dopamine reaction process rapidly decreased as the number of cycles increases, as shown in figures 7(a)–(c). It is believed that the products of dopamine oxidation were diffused and redeposited to P-CNF and PDA backbone structures covering the electrode. Figure 7(d) shows different scan rates for pure CNF, which indicated no significant change in the CV. Figure 7(e) represents different PDA concentrations in P-CNF:P-CNF1, P-CNF2, and P-CNF3, compared with the CNF and bare platinum electrodes. When the CNF coated on the bare platinum electrode, the CV curve area increased. When the PDA concentration increased, the CV curve area and the oxidation dopant peak near 0.4 V further increased. The increase was associated with the P-CNF coating.

The bare platinum electrode was CV tested as a reference and figure 8(a) shows its photograph, which showed a clear surface without any discoloration and poisoning electrode before and after CV tests. Figure 8(b) represents CNF electrode photograph, where CNF was uniformly coated on the electrode. Figures 8(c) and (d) show P-CNF3 electrode before and after CV test. It is assumed that the wrinkles of P-CNF3 deposited on the electrode might have resulted from the different affinity between the inert platinum and P-CNF3 layer. Further studies remain to analyze the properties change in the P-CNF layer by dopamine oxidation on the electrode. As illustrated in the CV analysis, the ion permeability control through the CNF backbone structure and oxidation process by PDA can provide unique functionality of flexible electrode materials for biomedical applications, in conjunction with the biocompatibility of CNF [51]. Also the conductive behavior with small capacitance of P-CNF electrode could be beneficial for biomedical electrode applications. The P-CNF electrode can have good interaction with biological objects for sending/receiving biological signals.

4. Conclusions

This article demonstrated a simple, fast, and eco-friendly route of fabricating considerably flexible and thermally stable PDA-CNF composites with electrochemical properties for flexible electrode material. The desired composites were successfully developed by controlled blending of PDA with CNF suspension. PDA concentration on the thermal, mechanical, and electrochemical behaviors of the composites was described explicitly. FTIR and XPS analysis endorsed the successful adhesion of PDA onto CNF. FESEM showed that PDA adhesion could significantly influence the interconnected network and layered structures of cellulose. The P-CNF composites showed a higher Young's modulus than pure PDA and slightly lower than pure CNF. The strain at break of the P-CNF composites increased as the PDA concentration increased, and over P-CNF2, it was somewhat decreased due to PDA aggregates. The toughness of the P-CNF composites showed a similar trend. The prepared P-CNF composite is flexible enough for biomedical electrode applications. CV analysis showed an ion permeability through the CNF backbone structure and oxidation process by PDA, which can provide unique functionality and biocompatibility for biomedical sensing. Combined with the improvement of the thermal stability, flexibility, the resulting electrochemical behavior of the P-CNF composites, and the simplicity and ecofriendly nature of the process, this work will be worthwhile for guiding the design of P-CNF composites aimed for biomedical electrodes and other sensing applications.

Acknowledgments

National Research Foundation of Korea supported this research through the Creative Research Initiatives Program (NRF-2015R1A3A2066301).

Conflicts of interest

The authors declare no conflict of interest.

ORCID iD

Jaehwan Kim https://orcid.org/0000-0002-6152-2924

References

- [1] Im C and Seo J-M 2016 A review of electrodes for the electrical brain signal recording *Biomed. Eng. Lett.* **6** 104–12
- [2] Polanco M, Bawab S and Yoon H 2016 Computational assessment of neural probe and brain tissue interface under transient motion *Biosensors* 6 27

- [3] Polikov V S, Tresco P A and Reichert W M 2005 Response of brain tissue to chronically implanted neural electrodes J. Neurosci. Methods 148 1–18
- [4] Xie Y, Martini N, Hassler C, Kirch R D, Stieglitz T, Seifert A and Hofmann U G 2014 *In vivo* monitoring of glial scar proliferation on chronically implanted neural electrodes by fiber optical coherence tomography *Front. Neuroeng.* 7 2–14
- [5] Altuna A, Berzango J and Fernandez L J 2015 Polymer SU-8-based microprobes for neural recording and drug delivery Front. Mater. 2 2
- [6] Wester B A, Lee R H and LaPlaca M C 2009 Development and characterization of *in vivo* flexible electrodes compatible with large tissue displacements *J. Neural. Eng.* 6 024002
- [7] Lee K, Singh A, He J, Massia S, Kim B and Raupp G 2004 Polyimide based neural implants with stiffness improvement Sensors Actuators B 102 67–72
- [8] Shen W, Karumbaiah L, Liu X, Saxena T, Chen S, Patkar R, Bellamkonda R V and Allen M G 2015 Extracellular matrix-based intracortical microelectrodes: toward a microfabricated neural interface based on natural materials *Microsyst. Nanoeng.* 1 15010
- [9] Altuna A, Menendez de la Prida L, Bellistri E, Gabriel G, Guimera A, Berganzo J, Villa R and Fernandez L J 2012 SU-8 based microprobes with integrated planar electrodes for enhanced neural depth recording *Biosens. Bioelectron.* 37 1–5
- [10] Lee K, He J, Clement R, Massia S and Kim B 2004 Biocompatible benzocyclobutene (BCB)-based neural implants with micro-fluidic channel *Biosens. Bioelectron*. 20 404–7
- [11] Lee S E, Jun S B, Lee H J, Kim J, Lee S W, Im C, Shin H, Chang J W and Kim S J 2012 A flexible depth probe using liquid crystal polymer *IEEE Trans. Biomed. Eng.* 59 2085–94
- [12] Nguyen J K, Park D J, Skousen J L, Hess-Dunning A E, Tyler D J, Rowan S J, Weder C and Capadona J R 2014 Mechanically-compliant intracortical implants reduce the neuroinflammatory response J. Neural. Eng. 11 056014
- [13] Sridharan A, Nguyen J K, Capadona J R and Muthuswamy J 2015 Compliant intracortical implants reduce strains and strain rates in brain tissue in vivo J. Neural. Eng. 12 036002
- [14] Gutowski S M, Shoemaker J T, Templeman K L, Wei Y, Latour R A, Bellamkonda R V, LaPlaca M C and García A J 2015 Protease-degradable PEG-maleimide coating with on-demand release of IL-1Ra to improve tissue response to neural electrodes *Biomaterials* 44 55–70
- [15] Kozai T D Y, Li X, Bodily L M, Caparosa E M, Zenonos G A, Carlisle D L, Friedlander R M and Cui X T 2014 Effects of caspase-1 knockout on chronic neural recording quality and longevity: insight into cellular and molecular mechanisms of the reactive tissue response *Biomaterials* 35 9620–34
- [16] Tsai D, Sawyer D, Bradd A, Yuste R and Shepard K L 2017 A very large-scale microelectrode array for cellular-resolution electrophysiology *Nat. Commun.* 8 1802
- [17] Rivnay J, Wang H, Fenno L, Deisseroth K and Malliaras G G 2017 Next-generation probes, particles, and proteins for neural interfacing Sci. Adv. 3 e1601649
- [18] Mao C, Zhang H and Lu Z 2017 Flexible and wearable electronic silk fabrics for human physiological monitoring Smart Mater. Struct. 26 095033
- [19] Tsai H-K A, Ma K-S, Wang C, Xu H, Wang C, Zoval J, Kulinsky L and Madou M 2007 Development of integrated protection for a miniaturized drug delivery system *Smart Mater. Struct.* 16 S295
- [20] Yang J-H, Cho H-S, Park S-H, Song S-H, Yun K-S and Lee J H 2016 Effect of garment design on piezoelectricity harvesting from joint movement *Smart Mater. Struct.* 25 035012

- [21] Li Y, Yong X, Cheung T and Menon C 2016 Compliant finger sensor for sensorimotor studies in MEG and MR environment Smart Mater. Struct. 25 075030
- [22] Kim J-H, Shim B S, Kim H S, Lee Y-J, Min S-K, Jang D, Abas Z and Kim J 2015 Review of nanocellulose for sustainable future materials *Int. J. Precis. Eng. Manuf. Green Techn.* 2 197–213
- [23] Zhang N, Zang G-L, Shi C, Yu H-Q and Sheng G-P 2016 A novel adsorbent TEMPO-mediated oxidized cellulose nanofibrils modified with PEI: preparation, characterization, and application for Cu(II) removal *J. Hazard. Mater*. 316 11–18
- [24] Moon R J, Martini A, Nairn J, Simonsen J and Youngblood J 2011 Cellulose nanomaterials review: structure, properties and nanocomposites *Chem. Soc. Rev.* 40 3941–94
- [25] Zhai L, Kim H C, Kim J W, Kang J and Kim J 2018 Elastic moduli of cellulose nanofibers isolated from various cellulose resources by using aqueous counter collision *Cellulose* 25 4261–8
- [26] Pattinson S W and Hart A J 2017 Additive manufacturing of cellulosic materials with robust mechanics and antimicrobial functionality Adv. Mater. Technol. 2 1600084
- [27] Huber T, Müssig J, Curnow O, Pang S, Bickerton S and Staiger M P 2012 A critical review of all-cellulose composites J. Mater. Sci. 47 1171–86
- [28] Kim H C, Mun S, Ko H-U, Zhai L, Kafy A and Kim J 2016 Renewable smart materials Smart Mater. Struct. 25 073001
- [29] Bashar M M, Zhu H, Yamamoto S and Mitsuishi M 2017 Superhydrophobic surfaces with fluorinated cellulose nanofiber assemblies for oil-water separation RSC Adv. 7 37168–74
- [30] Nechyporchuk O, Yu J, Nierstrasz V A and Bordes R 2017 Cellulose nanofibril-based coatings of woven cotton fabrics for improved inkjet printing with a potential in e-textile manufacturing ACS Sustain. Chem. Eng. 5 4793–801
- [31] Kim H C, Kim J W, Zhai L and Kim J 2019 Strong and tough long cellulose fibers made by aligning cellulose nanofibers under magnetic and electric fields *Cellulose* **26** 5821–9
- [32] Kafy A, Kim H C, Zhai L, Kim J W and Kang T J 2017 Cellulose long fibers fabricated from cellulose nanofibers and its strong and tough characteristics Sci. Rep. 7 1–8
- [33] Yang J, Du M, Wang L, Li S, Wang G, Yang X, Zhang L, Fang Y, Zheng W and Yang G 2018 Bacterial cellulose as a supersoft neural interfacing substrate ACS Appl. Mater. Interfaces 10 33049–59
- [34] Roy S, Das T, Zhang L and Hu X M 2016 Harnessing the maximum reinforcement of graphene oxide for poly (vinylidene fluoride) nanocomposites via polydopamine assisted novel surface modification RSC Adv. 6 69919–29
- [35] Su Y, Zhao Y, Zhang H, Feng X, Shi L and Fang J 2016 Polydopamine functionalized transparent conductive cellulose nanopaper with long-term durability *J. Mater. Chem.* C 5 573–81
- [36] Lee H, Dellatore S M, Miller W M and Messersmith P B 2007 Mussel-inspired surface chemistry for multifunctional coatings Science 318 426–30
- [37] Zhang L, Roy S, Chen Y, Chua E K, See K Y, Hu X and Liu M 2014 Mussel-inspired polydopamine coated hollow carbon microspheres, a novel versatile filler for fabrication of high performance syntactic foams ACS Appl. Mater. Interfaces 6 18644–52
- [38] Subramanian A S, Tey J N, Zhang L, Ng B H, Roy S and Wei J 2016 Synergistic bond strengthening in epoxy adhesives using polydopamine/MWCNT hybrids *Polymer* 82 285–94
- [39] Ou J, Wang J, Zhou J, Liu S, Yu Y, Pang X and Yang S 2010 Construction and study on corrosion protective property of polydopamine-based 3-layer organic coatings on aluminum substrate *Prog. Org. Coat.* 68 244–7

- [40] Jiang J, Zhang P, Zhu L, Zhu B and Xu Y 2015 Improving antifouling ability and hemocompatibility of poly (vinylidene fluoride) membranes by polydopamine-mediated ATRP J. Mater. Chem. B 3 7698–706
- [41] Roy S, Kuddannaya S, Das T, Lee H Y, Lim J, Yoon Y C and Kim J 2017 A novel approach for fabricating highly tunable and fluffy bioinspired 3D poly (vinyl alcohol) (PVA) fiber scaffolds *Nanoscale* 9 7081–93
- [42] Toma M and Tawa K 2017 Thickness dependence of polydopamine thin films on detection sensitivity of surface plasmon-enhanced fluorescence biosensors *Japan J. Appl. Phys.* 57 03EK01
- [43] Nishida H and Koga F 2018 Potential of oxidative polymerization coating of cellulose nanofiber by dopamine *Mater. Sci. Eng.* 368 012043
- [44] Hong G, Meng Y, Yang Z, Cheng H, Zhang S and Song W 2017 Mussel-inspired polydopamine modification of bamboo fiber and its effect on the properties of bamboo fiber/polybutylene succinate composites *BioResources* 12 8419–42
- [45] Li Y, Wang B, Sui X, Xu H, Zhang L, Zhong Y and Mao Z 2017 Facile synthesis of microfibrillated cellulose/organosilicon/polydopamine composite sponges with flame retardant properties Cellulose 24 3815–23
- [46] Furtado L M, Ando R A and Petri D F S 2020 Polydopamine-coated cellulose acetate butyrate microbeads for caffeine removal J. Mater. Sci. 55 3243–58
- [47] Ang M B M Y, Macni C R M, Caparanga A R, Huang S-H, Tsai H-A, Lee K-R and Lai J-Y 2020 Mitigating the fouling of mixed-matrix cellulose acetate membranes for oil-water separation through modification with polydopamine particles *Chem. Eng. Res. Des.* 159 195–204
- [48] Cui Z, Lin J, Zhan C, Wu J, Shen S, Si J and Wang Q 2020 Biomimetic composite scaffolds based on surface modification of polydopamine on ultrasonication induced cellulose nanofibrils (CNF) adsorbing onto electrospun thermoplastic polyurethane (TPU) nanofibers *J. Biomater. Sci., Polym. Ed.* 31 561–77
- [49] Wang G, Zhang J, Lin S, Xiao H, Yang Q, Chen S, Yan B and Gu Y 2020 Environmentally friendly nanocomposites based on cellulose nanocrystals and polydopamine for rapid removal of organic dyes in aqueous solution *Cellulose* 27 2085–97
- [50] Dong L, Deng R, Xiao H, Chen F, Zhou Y, Li J, Chen S and Yan B 2019 Hierarchical polydopamine coated cellulose nanocrystal microstructures as efficient nanoadsorbents for removal of Cr (VI) ions Cellulose 26 6401–14

- [51] Wang L, Zhu H, Xu G, Hou X, He H and Wang S 2020 A biocompatible cellulose-nanofiber-based multifunctional material for Fe 3+ detection and drug delivery *J. Mater. Chem.* C 8 11796–804
- [52] Yang L, Chen C, Hu Y, Wei F, Cui J, Zhao Y, Xu X, Chen X and Sun D 2020 Three-dimensional bacterial cellulose/polydopamine/TiO₂ nanocomposite membrane with enhanced adsorption and photocatalytic degradation for dyes under ultraviolet-visible irradiation *J. Colloid Interface Sci.* 562 21–8
- [53] Cui J, Xu X, Yang L, Chen C, Qian J, Chen X and Sun D 2020 Soft foam-like UiO-66/polydopamine/bacterial cellulose composite for the removal of aspirin and tetracycline hydrochloride *Chem. Eng. J.* 350 125174
- [54] Klosterman L, Ahmad Z, Viswanathan V and Bettinger C J 2017 Synthesis and measurement of cohesive mechanics in polydopamine nanomembranes Adv. Mater. Interfaces 4 1700041
- [55] Li H, Xi J, Zhao Y and Ren F 2019 Mechanical properties of polydopamine (PDA) thin films MRS Adv. 4 405–12
- [56] Mallinson D, Mullen A B and Lamprou D A 2018 Probing polydopamine adhesion to protein and polymer films: microscopic and spectroscopic evaluation *J. Mater. Sci.* 53 3198–209
- [57] Kumar A, Negi Y S, Choudhary V and Bhardwaj N K 2014 Characterization of cellulose nanocrystals produced by acid-hydrolysis from sugarcane bagasse as agro-waste *J. Mater. Phys. Chem.* 2 1–8
- [58] Xu C, Zhu S, Xing C, Li D, Zhu N and Zhou H 2015 Isolation and properties of cellulose nanofibrils from coconut palm petioles by different mechanical process *PLoS One* 10 e0122123
- [59] Lin S, Chen C-T, Bdikin I, Ball V, Grácio J and Buehler M J 2014 Tuning heterogeneous poly (dopamine) structures and mechanics: in silico covalent cross-linking and thin film nanoindentation Soft Matter 10 457–64
- [60] Hai L V, Zhai L, Kim H C, Kim J W, Choi E S and Kim J 2018 Cellulose nanofibers isolated by TEMPO-oxidation and aqueous counter collision methods *Carbohydr. Polym.* 191 65–70
- [61] Saito T, Kimura S, Nishiyama Y and Isogai A 2007 Cellulose nanofibers prepared by TEMPO-mediated oxidation of native cellulose *Biomacromolecules* 8 2485–91
- [62] Kondo T, Kose R, Naito H and Kasai W 2014 Aqueous counter collision using paired water jets as a novel means of preparing bio-nanofibers *Carbohydr. Polym.* 112 284–90